Chapter 5

Uniform global feedback — Theoretical part

In this chapter, control of chemical turbulence in oscillatory reaction-diffusion systems is investigated theoretically. This study is motivated in particular by the experimental results presented in Section 4.2: Although the magnitude of the feedback signal could be reduced considerably, it was found in the experiment that the ideal limit of a vanishingly small feedback signal in the state of control could not be reached. In the following, the behavior of the experimental system will be analyzed in terms of specific as well as more general models for oscillatory systems. Both analytical arguments and numerical simulations are employed to explain the experimental results and to establish an overall understanding of the behavior of extended oscillatory systems under global delayed feedback. The chapter consists of two parts. In Section 5.1, the spatial degrees of freedom are neglected and the homogeneous dynamics of an oscillatory system is studied in the presence of global delayed feedback. In Section 5.2, a spatially extended system is considered and the stability of uniform oscillations is analyzed for the complex Ginzburg-Landau equation with global feedback.

5.1 Homogeneous dynamics

In Section 4.2, experimental results were presented showing that efficient control of chemical turbulence can be achieved by implementing global delayed feedback and optimizing the delay time in the control scheme (time-delay autosynchronization, TDAS).

For a complete understanding of this process it is necessary to consider the dynamics of a spatially extended system in the presence of feedback. However, once turbulence is suppressed and uniform oscillations are established, diffusive coupling can be neglected and the dynamics is reduced to the behavior of a single oscillator.

In this section, the dynamics of a uniformly oscillating system is discussed. Stability of uniform oscillations with respect to spatial perturbations is not considered here and will be analyzed later (Section 5.2). The phase dynamics equation of a single oscillator in the presence of weak feedback is analyzed and numerical simulations using the realistic reaction model of catalytic CO oxidation on Pt(110) are presented to complement the analytical results.

5.1.1 Phase dynamics equation

In many cases, the dynamics of an oscillatory system can be described in terms of a single phase variable only. For introductory remarks on phase dynamics approximations see Section 2.4.2. In the case of weak feedback, a separation of time scales may occur between the amplitude and phase variables allowing adiabatic elimination of the amplitude variable. Thus, a phase dynamics equation can be obtained that involves the oscillation phase ϕ as the only dynamical variable. The phase equation of a single oscillator under the effect of weak TDAS takes the form

$$\dot{\phi} = \omega + \mu f(\phi(t) - \phi(t-\tau)) \,, \tag{5.1}$$

see also Ref. [217]. Here, ω is the oscillation frequency in absence of feedback, τ is the delay time, and μ is the coefficient characterizing the feedback intensity (note that the phase equation is only valid for $\mu \ll 1$). The exact form of the function $f(\phi(t)-\phi(t-\tau))$ depends on the specific system under consideration. Generally, f is 2π-periodic and satisfies the conditions $f(0) = f(2\pi) = 0$. As an example, the derivation of Eq. (5.1) is shown in Appendix C for the Stuart-Landau equation (2.21) with additional TDAS feedback term. In this case, the function f is given by

$$f(\Delta\phi) = a \, \sin(\Delta\phi) + b \, \cos(\Delta\phi) - b \,, \tag{5.2}$$

with $\Delta\phi = \phi(t) - \phi(t-\tau)$, $a = \cos\chi + \beta\sin\chi$, and $b = \sin\chi - \beta\cos\chi$. The parameters β and χ are the coefficients of the Stuart-Landau equation with TDAS (see Appendix C).

Solutions In the state of control, the experimental system performs periodic uniform oscillations. In the simplified phase model introduced above, these oscillatory states correspond to harmonic solutions of the phase equation (5.1) that are of the form $\phi(t) = \Omega t$. Their oscillation frequency $\dot{\phi} = \Omega$ should satisfy

$$\Omega = \omega + \mu f(\Omega\tau)\,. \tag{5.3}$$

The solutions can be constructed by rewriting Eq. (5.3) in the following way,

$$\mu = \frac{\Omega - \omega}{f(\Omega\tau)}\,. \tag{5.4}$$

For each oscillation frequency Ω, Eq. (5.4) determines the respective value of the feedback intensity μ at a given delay time τ. Figure 5.1 shows the solutions of Eq. (5.3) as

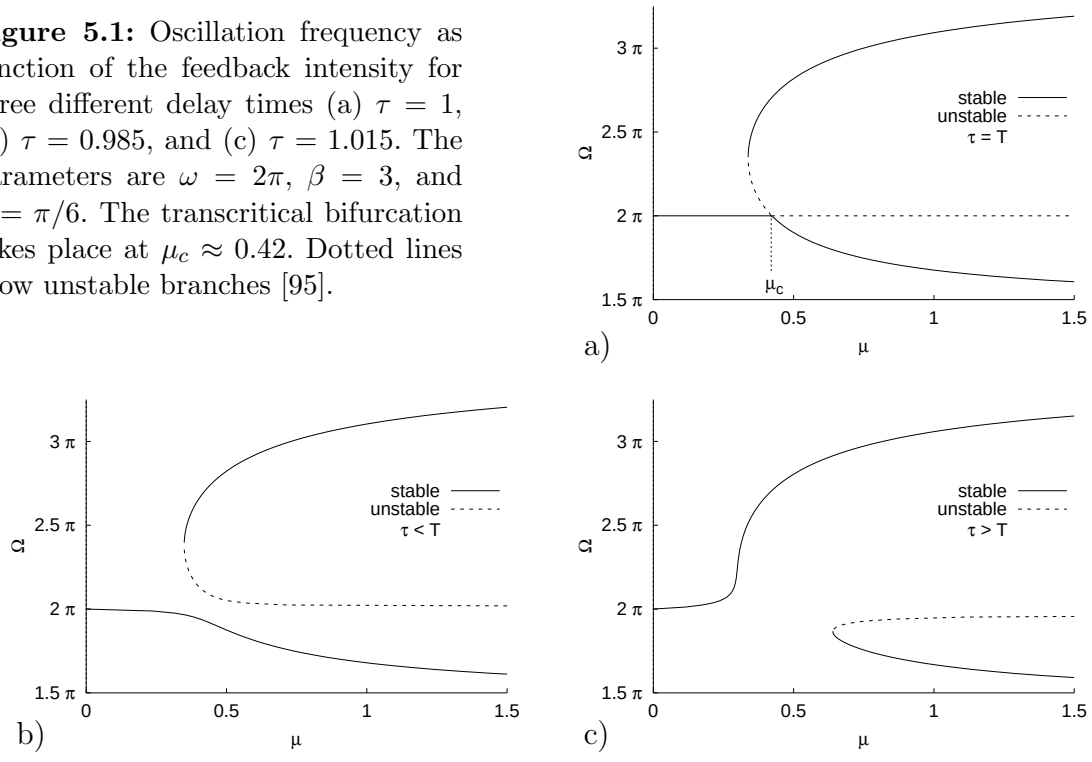

Figure 5.1: Oscillation frequency as function of the feedback intensity for three different delay times (a) $\tau = 1$, (b) $\tau = 0.985$, and (c) $\tau = 1.015$. The parameters are $\omega = 2\pi$, $\beta = 3$, and $\chi = \pi/6$. The transcritical bifurcation takes place at $\mu_c \approx 0.42$. Dotted lines show unstable branches [95].

a function of the feedback intensity for three different delay times. As an example, the function f is chosen as in Eq. (5.2) with $\beta = 3$ and $\chi = \pi/6$.

When the delay time is equal to the natural oscillation period, $\tau = T_0 = 2\pi/\omega$, Eq. (5.3) has always a solution $\Omega = \omega$ with vanishing feedback signal. However, other solutions are additionally present at sufficiently high feedback intensities, as seen in Fig. 5.1 (a). They emerge via a saddle-node bifurcation. For these solutions, $\Omega \neq \omega$ and the feedback signal is not vanishing. The solution with $\Omega = \omega$ intersects with the other solutions in a transcritical bifurcation at $\mu = \mu_c$. Generally, the bifurcation point is given by

$$\mu_c = \lim_{\Omega \to \omega} \frac{\Omega - \omega}{f(2\pi \frac{\Omega}{\omega})} = \frac{\omega}{2\pi f'(0)} \,. \tag{5.5}$$

When $\tau \neq T$, the situation is different. No transcritical bifurcation occurs. Only a saddle-node bifurcation is found, leading to the appearance of two new solution branches at sufficiently high feedback intensities, as shown in Figs. 5.1 (b) and (c).

Stability The linear stability of the different solutions of Eq. (5.1) can be analyzed by simple considerations. Suppose a small perturbation $\delta\phi$ is applied to the phase. Substituting $\phi = \Omega t + \delta\phi$ into Eq. (5.1), the following equation for $\delta\phi$ is obtained after linearization,

$$\dot{\delta\phi} = \mu f'(\Omega\tau)(\delta\phi(t) - \delta\phi(t-\tau)) \,. \tag{5.6}$$

With an ansatz $\delta\phi(t) = e^{\lambda t/\tau}$, Eq. (5.6) yields

$$\lambda = q\,(1 - e^{-\lambda}) \,, \tag{5.7}$$

where $q = \tau\mu f'(\Omega\tau)$. The solution with frequency Ω is stable, if Re $\lambda < 0$. Here, the stability of the solution with vanishing feedback, $\Omega = \omega$, that occurs when $\tau = T_0$, is of particular interest. In this case, the coefficient q can be written as

$$q = \frac{\mu}{\mu_c} \tag{5.8}$$

by taking into account (5.5) and $f'(\Omega\tau) = f'(2\pi) = f'(0)$. Analyzing the roots of the characteristic equation (5.7), it can be shown that the solution with $\Omega = \omega$ becomes

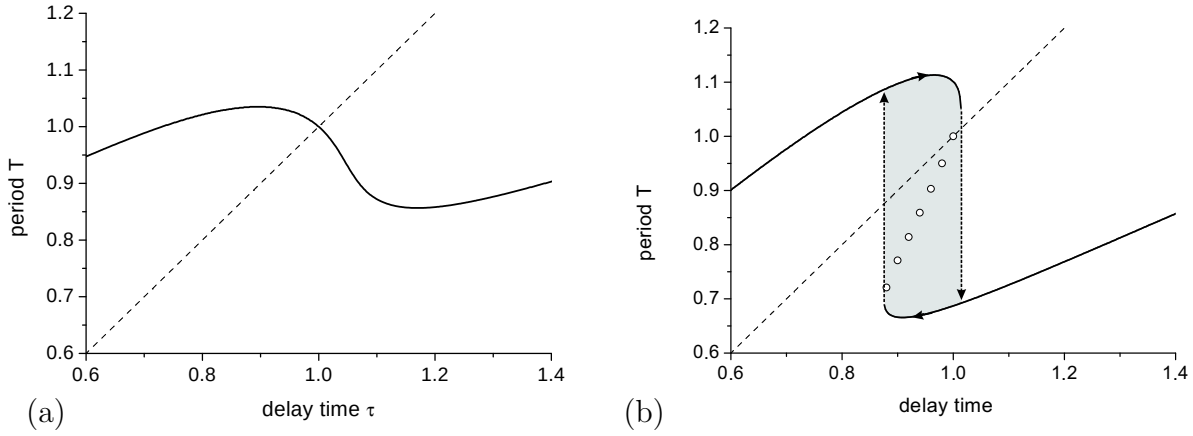

Figure 5.2: Oscillation period as function of delay time in the phase dynamics equation (5.1). (a) $\mu = 0.2$ and (b) $\mu = 0.6$. The other parameters are as in Fig. 5.1. Hysteresis effects are found in the gray shaded region in (b). Open circles indicate unstable solutions yielded by Eq. (5.3). Time step for integration $\Delta t = 0.0001$ [95].

unstable at the transcritical bifurcation point $\mu = \mu_c$. A similar analysis can be performed for the other solution branches and also for $\tau \neq T$. As a result, it is found that the branches indicated by solid (dotted) lines in Fig. 5.1 are stable (unstable).

In summary, the phase dynamics equation of a single oscillator in the presence of TDAS predicts that for $\tau = T_0$ a solution with vanishing feedback, $\Omega = \omega$, is present and becomes unstable at sufficiently high feedback intensities. It will be replaced by one of the two possible solutions with $\Omega \neq \omega$ and a nonvanishing feedback signal.

Numerical simulations To confirm the analytical results, a series of numerical simulations of Eq. (5.1) is performed tracing the oscillation period $T = 2\pi/\Omega$ as a function of the delay time τ. Figure 5.2 (a) displays the dependence of T on the delay time τ for a feedback intensity below the critical value (for $\mu < \mu_c$). Obviously, at $\tau = T_0$, the solution with $\Omega = \omega$ is indeed stable. However, if the feedback intensity is increased above the critical value μ_c, the solution for which $\tau = T$ is unstable and a state with vanishing feedback signal cannot be established. Instead, a discontinuity occurs if T is recorded as a function of τ and hysteresis can be observed, see Fig. 5.2 (b).

Comparing Fig. 5.2 and Fig. 4.7, it can be seen that the change of the oscillation period under varying delay time is qualitatively similar in the experiment and in the numerical

simulations based on the phase dynamics equation with $\mu > \mu_c$. However, it is pointed out that the phase equation is strictly valid only for weak feedbacks. Therefore, an analysis of the behavior at stronger feedbacks requires additional simulations based on a realistic reaction model.

5.1.2 Realistic reaction model

The temporal behavior of catalytic CO oxidation on Pt(110) single crystal surfaces is well described by a realistic model of three coupled ordinary differential equations for the dynamics of the CO coverage, the O coverage, and the fraction of the surface found in the nonreconstructed 1×1 phase, respectively. The model Eqs. (2.7)–(2.9) were introduced and discussed in Section 2.2.4.

Here, the model is extended by an additional equation taking into account the presence of delayed feedback. Similar to the experiment, the feedback induces temporal changes in the CO partial pressure depending on the evolution of the adsorbate coverages on the catalytic surface. For simplicity, the coupling is introduced via a dependence of the CO partial pressure on the CO coverage,

$$p_{\mathrm{CO}}(t) = p^0_{\mathrm{CO}} + \mu(u(t-\tau) - u(t))\,, \tag{5.9}$$

where p^0_{CO} is the base CO partial pressure, μ is the feedback intensity, and τ is the delay time. Note that Eq. (5.9) is only a qualitative approximation of the experimental setup described by Eq. (4.2). In the experiment, the feedback signal was generated based on the integral intensity I of the PEEM image. The image intensity I shows a nonlinear dependence on both the CO and the O coverage and the exact functional form of this relation is not known [94]. However, the simplified modeling according to Eq. (5.9) has been successfully applied in many situations, see *e.g.* Refs. [57, 79, 216].

Numerical simulations of the model (2.7)–(2.9), (5.9) are performed using a set of parameters for which the medium is in the oscillatory state and, if mobility of adsorbed CO molecules had been taken into account, diffusion-induced turbulence would have spontaneously developed. For the values of the model parameters see the caption of Fig. 5.3. The period of oscillations in absence of feedback is $T_0 = 2.44$ s.

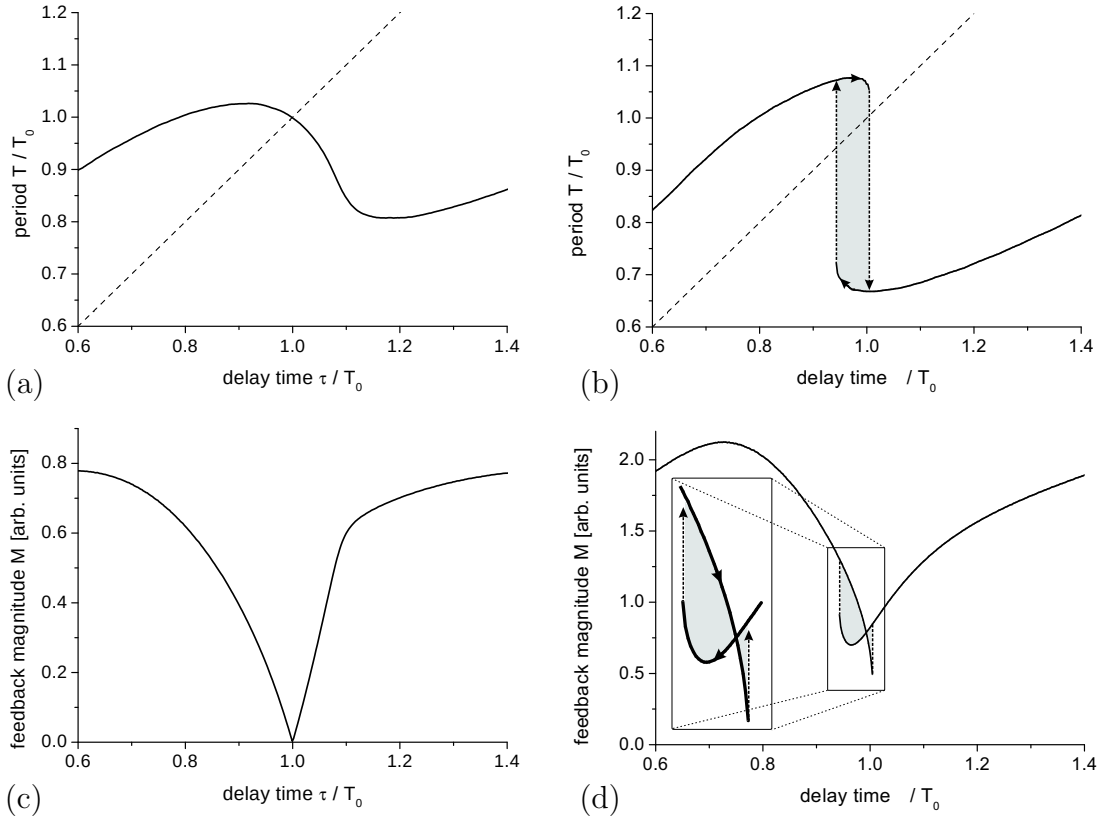

Figure 5.3: Oscillation period (a,b) and feedback magnitude (c,d) as functions of the delay time τ obtained from numerical simulations of the realistic model of CO oxidation on Pt(110) for two different feedback intensities (a,c) $\mu/p^0_{\mathrm{CO}} = 0.01$ and (b,d) $\mu/p^0_{\mathrm{CO}} = 0.03$. The model parameters are $k_1 = 3.14 \times 10^5\,\mathrm{s^{-1}mbar^{-1}}$, $k_2 = 10.21\,\mathrm{s^{-1}}$, $k_3 = 283.8\,\mathrm{s^{-1}}$, $k_4 = 5.86 \times 10^5\,\mathrm{s^{-1}mbar^{-1}}$, $k_5 = 1.61\,\mathrm{s^{-1}}$, $s_{\mathrm{CO}} = 1.0$, $s_{\mathrm{O,1\times1}} = 0.6$, $s_{\mathrm{O,1\times2}} = 0.4$, $u_0 = 0.35$, $\delta u = 0.05$, $p^0_{\mathrm{CO}} = 4.82 \times 10^{-5}\mathrm{mbar}$, and $p_{\mathrm{O_2}} = 13.1 \times 10^{-5}\mathrm{mbar}$. Time step for integration $\Delta t = 0.001\,\mathrm{s}$ [95].

Figure 5.3 shows the results of numerical simulations of the realistic model. Here, the dependences of the oscillation period T and of the feedback magnitude $M = \langle |u(t-\tau) - u(t)| \rangle$ on the delay time τ are displayed. For relatively weak feedback, a state with vanishing feedback signal M is realized at $\tau = T_0$, see Fig. 5.3 (a) and (c). When the feedback is increased, this state, however, becomes unstable and cannot be reached in simulations. Instead, hysteresis is observed as shown in Fig. 5.3 (b) and (d). Starting with short delay times and increasing τ, the oscillation period T gradually grows. When the delay time becomes slightly larger than T_0, the oscillation period abruptly jumps down to a value below T_0 and then slowly increases again. When moving in the opposite direction and gradually decreasing the delay time, a jump to

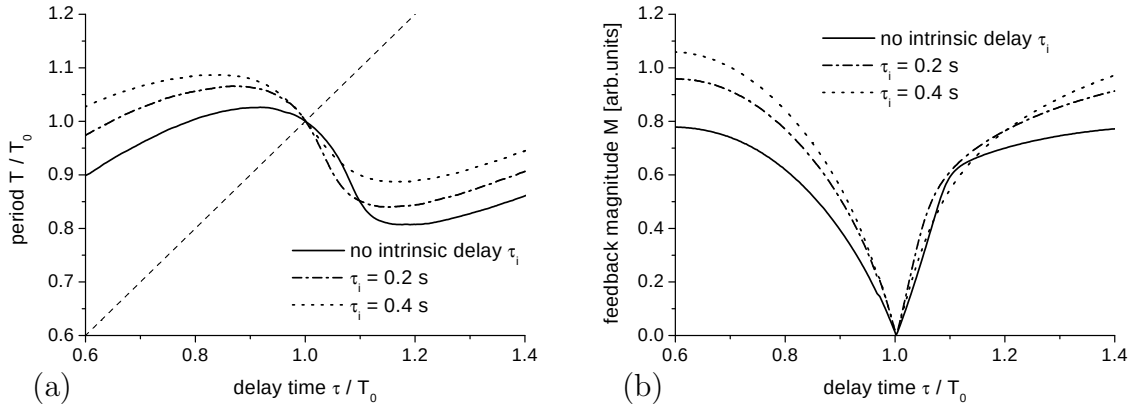

Figure 5.4: Effects of control loop latency: (a) oscillation period and (b) feedback magnitude as function of delay time for different values of intrinsic delay. The model parameters and time step as in Fig. 5.3 (a) and (c) [95].

the upper branch occurs slightly below $\tau = T_0$. Though the feedback magnitude is decreased when the value of τ lies in the vicinity of T_0, it does not drop down to zero here and a hysteresis effect for this quantity is also observed, see Fig. 5.3 (d).

Control loop latency In Section 4.2.1, it was pointed out that the feedback signal takes effect with an additional time delay τ_i in the experiments. This intrinsic delay is determined by the finite pumping rate of the reactor and cannot be eliminated completely for technical reasons. It is known from both experimental [218] and theoretical [219] studies that a control loop latency in the application of TDAS-type feedbacks might affect the size of the domain of control of the system. Here, however, the domain of control and its extension is not analyzed. The present investigation is rather focused on a qualitative explanation of the behavior in the state of control for different delay times. In order to study the impact of control loop latency on the results presented above, the computations shown in Fig. 5.3 (a) and (c) are repeated including an additional intrinsic delay τ_i. To this end, the model equations were modified taking into account the effect of a finite pumping rate on the time evolution of the CO partial pressure,

$$\dot{p}_{\mathrm{CO}} = \frac{1}{\tau_i}[\, p^0_{\mathrm{CO}} + \mu(u(t-\tau) - u(t)) - p_{\mathrm{CO}}]\,. \tag{5.10}$$

Figure 5.4 shows (a) the oscillation period T and (b) the feedback magnitude M as a function of delay time τ for two different values of the intrinsic delay τ_i in comparison

to the results for zero intrinsic delay which are, of course, identical to Fig. 5.3 (a) and (c). With increasing intrinsic delay, the curve describing the dependence of the oscillation period on the delay time experiences a shift to higher values but maintains its original shape. The change in the feedback magnitude, on the other hand, consists roughly in an increase by some factor larger one. However, both the oscillation period and the feedback magnitude maintain qualitatively similar shapes in their dependence on τ for both vanishing and non-zero τ_i. In particular, it is pointed out that the effect of control loop latency does not simply amount to adding up the intrinsic delay τ_i and the delay τ from the control scheme. Instead, the intersection point of the curve giving the dependence of T on τ with the line for which $T = \tau$ is not shifted when control loop latency is introduced and, as a consequence, the minimum of the feedback magnitude remains at the same position as well. Moreover, the effect of intrinsic delay gets less pronounced when approaching the point $T = \tau$, which is of particular interest for the present investigation.

5.2 Extended system

Chemical turbulence is a spatiotemporal phenomenon. In many systems where the local dynamics is nonchaotic, spatial coupling between a large number of individual elements is the key prerequisite for the emergence of turbulence (*e.g.* diffusion-induced turbulence). For an overall understanding of turbulence control by global feedback it is therefore essential to consider a spatially extended system.

In the previous section, the temporal behavior of a uniform system under global delayed feedback was studied. This analysis is now extended by taking spatial degrees of freedom into account. In particular, the stability of uniform oscillations with respect to spatial perturbations will be investigated in the presence of a TDAS-type feedback. As a general model for spatially extended oscillatory systems, the complex Ginzburg-Landau equation (CGLE) is chosen. The CGLE was introduced in Section 2.4.1 and its basic properties were briefly discussed. Here, the CGLE is extended by an additional global TDAS feedback term,

$$\dot{\eta} = (1 - i\omega)\eta - (1 + i\beta)|\eta|^2\eta + (1 + i\varepsilon)\nabla^2\eta + F(t)\,, \tag{5.11}$$

where $F(t)$ is given by

$$F(t) = \mu\, e^{i\chi}(\bar{\eta}(t - \tau) - \bar{\eta}(t)) \qquad \text{with} \qquad \bar{\eta}(t) = \frac{1}{L}\int_0^L \eta(x, t)\mathrm{d}x\,. \tag{5.12}$$

The parameters μ, τ, and χ denote the feedback intensity factor, the delay time, and a phase shift in the application of the control force, respectively.

In the following, linear stability of uniform oscillations in the presence of TDAS is analyzed and a synchronization diagram in the plane spanned by the feedback parameters is derived. Numerical simulations of the CGLE with TDAS are performed to verify the analytical results and to give examples of additional space-time phenomena at the border of synchronization. They are presented in Section 5.2.2.

5.2.1 Linear stability analysis

In the absence of feedback ($F = 0$), uniform oscillations are unstable if the Benjamin-Feir condition is fulfilled, $(1 + \varepsilon\beta) < 0$, and an irregular turbulent state develops. By application of global delayed feedback, turbulence can be suppressed and uniform oscillations are stabilized. In this section, the stability of uniform oscillations is examined as a function of the feedback parameters. Small spatially inhomogeneous perturbations are applied to the uniform state and the growth rates of these nonuniform modes are analyzed.

Consider a superposition of the homogeneous mode H with a small spatially inhomogeneous perturbation of arbitrary non-zero wave number κ,

$$\eta(x,t) = H(t) + A_+(t)e^{i\kappa x} + A_-(t)e^{-i\kappa x}\,. \tag{5.13}$$

Substituting expression (5.13) into Eq. (5.11) and assuming that the amplitudes $A_\pm$ of the perturbation are small, homogeneous contributions can be separated from spatially inhomogeneous terms. In this way, an equation for the homogeneous mode is found which is decoupled from the nonuniform contributions,

$$\dot{H} = (1 - i\omega)H - (1 + i\beta)|H|^2H + \mu e^{i\chi}(H(t-\tau) - H(t))\,. \tag{5.14}$$

The behavior of the wave amplitudes $A_\pm$ is governed by a pair of coupled equations

$$\dot{A}_+ = (1 - i\omega)A_+ - (1 + i\varepsilon)\kappa^2 A_+ - 2(1 + i\beta)|H|^2A_+ - (1 + i\beta)H^2A_-^*, \tag{5.15}$$

$$\dot{A}_-^* = (1 + i\omega)A_-^* - (1 - i\varepsilon)\kappa^2 A_-^* - 2(1 - i\beta)|H|^2A_-^* - (1 - i\beta)H^{*2}A_+. \tag{5.16}$$

Stability of the uniform system In Section 5.1.1, the stability of a uniform oscillatory system under delayed feedback was discussed in the general context of a phase dynamics equation. Although the results agree with the prediction of the phase model, the uniform dynamics of the system considered in this section will be presented here for completeness. The evolution of the uniform mode is described by Eq. (5.14) which represents a Stuart-Landau equation with an additional global feedback term. Substituting $H = \rho_0\, e^{-i\Omega t}$ into Eq. (5.14) the amplitude of uniform oscillations in the presence

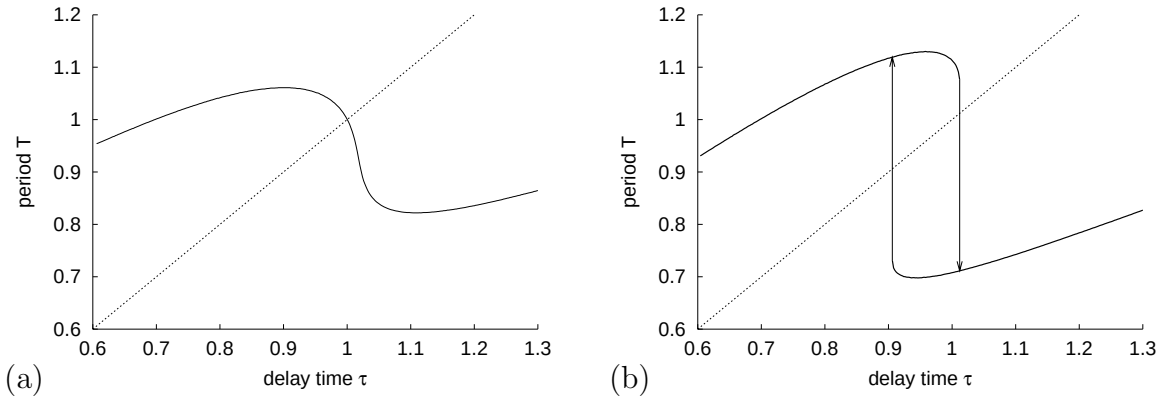

Figure 5.5: Oscillation period as a function of delay time in numerical integrations of Eq.(5.14). (a) $\mu = 0.5$ and (b) $\mu = 1.0$. Parameters: $\beta = -1.4$, $\omega = 2\pi - \beta \approx 7.68$, and $\chi = \pi/2$. Time step for integration $\Delta t = 0.0001$ [220].

of TDAS is obtained,

$$\rho_0 = \sqrt{1 + \mu(\cos(\chi + \Omega\tau) - \cos\chi)}\,, \tag{5.17}$$

and an equation for the frequency Ω of uniform oscillations can be derived,

$$\Omega = \omega + \beta + \mu\beta(\cos(\chi + \Omega\tau) - \cos\chi) - \mu(\sin(\chi + \Omega\tau) - \sin\chi)\,. \tag{5.18}$$

Note that in absence of feedback ($\mu = 0$) the system shows uniform oscillations with the frequency $\Omega_0 = \omega + \beta$.

Figure 5.5 shows the results of numerical integrations of Eq. (5.14). The oscillation period $T = 2\pi/\Omega$ is displayed as a function of the delay time τ in the case of weak (a) and strong (b) feedback. The state with $T = \tau$ is stable for weak feedback and becomes unstable with increasing feedback intensity.

The stability of the intersection point for which $T = \tau$ can be understood in terms of the bifurcation diagram presented in Fig. 5.6. This diagram is constructed by solving Eq. (5.18) for a delay time τ equal to the period $T_0 = 2\pi/(\omega + \beta)$ of oscillations in the nonperturbed uniform system. Besides a solution with a vanishing feedback term, for which $\Omega = \Omega_0$, other solutions with a non-zero feedback and $\Omega \neq \Omega_0$ are obtained from Eq. (5.18). The solution with $\Omega = \Omega_0$ and a vanishing feedback is stable for small μ and becomes unstable beyond some critical feedback intensity μ_0. Both the results from

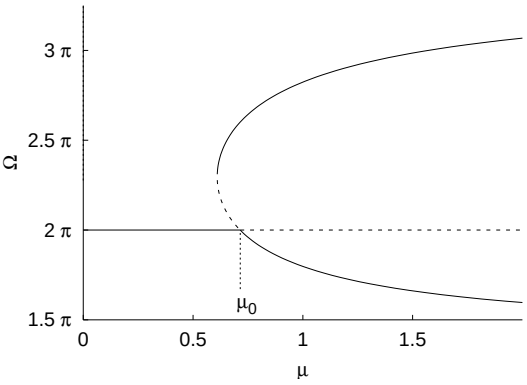

Figure 5.6: Bifurcation diagram for $\tau = T_0 = 1$. The parameters are as in Fig. 5.5. Dotted lines denote unstable branches. The uniform solution with $\Omega = \Omega_0 = 2\pi$ and a vanishing feedback signal undergoes a transcritical bifurcation at $\mu = \mu_0$ and becomes unstable [220].

the numerical simulations shown in Fig. 5.5 and the bifurcation diagram in Fig. 5.6 are in close agreement with the behavior predicted by the phase model in the previous section.

Stability of uniform oscillations in the spatially extended system We now turn to the stability analysis of uniform oscillations with respect to spatially inhomogeneous perturbations. In general, Eqs. (5.15) and (5.16) for the spatially nonuniform contributions can be written in the form

$$\dot{A}_+ = aA_+ + be^{-i2\Omega t}A_-^* \,, \tag{5.19}$$

$$\dot{A}_-^* = a^*A_-^* + b^*e^{i2\Omega t}A_+ \,. \tag{5.20}$$

By a simple change of variables, $A_+ = \tilde{A}_+e^{-i\Omega t}$ and $A_-^* = \tilde{A}_-^*e^{i\Omega t}$, Eqs. (5.19) and (5.20) transform into

$$\dot{\tilde{A}}_+ = \tilde{a}\tilde{A}_+ + b\tilde{A}_-^* \,, \tag{5.21}$$

$$\dot{\tilde{A}}_-^* = \tilde{a}^*\tilde{A}_-^* + b^*\tilde{A}_+ \,, \tag{5.22}$$

with $\tilde{a} = a + i\Omega$. To solve this system of equations, we substitute the ansatz $\tilde{A}_+ = \tilde{A}_+^0 e^{\lambda t}$ and $\tilde{A}_-^* = \tilde{A}_-^{*0}e^{\lambda t}$ into the Eqs. (5.21) and (5.22) and obtain the following solutions for the eigenvalue λ,

$$\begin{aligned}\lambda_{1,2} &= \frac{\tilde{a}+\tilde{a}^*}{2} \pm \sqrt{bb^* - \tilde{a}\tilde{a}^* + \frac{(\tilde{a}+\tilde{a}^*)^2}{4}} \\ &= 1 - \kappa^2 - 2\rho_0^2 \pm \sqrt{(1+\beta^2)\rho_0^4 - (\Omega - \omega - \varepsilon\kappa^2 - 2\beta\rho_0^2)^2} \,,\end{aligned} \tag{5.23}$$

where ρ_0 is given by Eq. (5.17) and Ω is a solution of Eq. (5.18). Uniform oscillations are stable with respect to the growth of spatially nonuniform modes if $\mathrm{Re}\,\lambda_{1,2} < 0$ for all wave numbers κ. The instability boundary is therefore determined by the conditions

$$\mathrm{Re}\,\lambda(\mu_c, \kappa_c) = 0\,, \tag{5.24}$$

$$\frac{\partial}{\partial\kappa}\,\mathrm{Re}\,\lambda(\mu_c, \kappa_c) = 0\,, \tag{5.25}$$

where μ_c denotes the critical feedback intensity and κ_c the wave number of the most unstable mode. Equation (5.25) accounts for the fact that the wave number of the first unstable mode corresponds to a maximum in λ plotted as a function of κ. The Eqs. (5.24) and (5.25) can be solved numerically, taking into account Eq. (5.18) for the dependence of the frequency Ω of the uniform mode on the feedback intensity μ and the delay time τ.

Invasiveness of the control scheme For the choice of $\tau = 2\pi/\Omega_0$ the analysis of the uniform case has shown that there is a solution of frequency $\Omega = \Omega_0 = \omega + \beta$ for which the feedback signal is vanishing so that control would be completely noninvasive. Moreover, it was found that this solution becomes unstable if the feedback intensity μ is increased above the threshold μ_0. On the other hand, considering a spatially extended system in the Benjamin-Feir unstable regime, it is obvious that a certain critical feedback intensity μ_c is necessary in order to suppress turbulence and to maintain uniform oscillations in the system. For $\tau = T_0$ and $\Omega = \Omega_0$ the general expression (5.23) for λ turns into

$$\lambda_{1,2} = -\kappa^2 - 1 \pm \sqrt{-\varepsilon^2\kappa^4 - 2\beta\varepsilon\kappa^2 + 1}\,, \tag{5.26}$$

which is independent of μ. Figure 5.7 shows a plot of the real part of λ as a function of wave number in the Benjamin-Feir stable and unstable regime and at the border of stability. In the Benjamin-Feir unstable case, all inhomogeneous modes with a wave number less than

$$\kappa = \sqrt{-\frac{2(1+\varepsilon\beta)}{1+\varepsilon^2}} \tag{5.27}$$

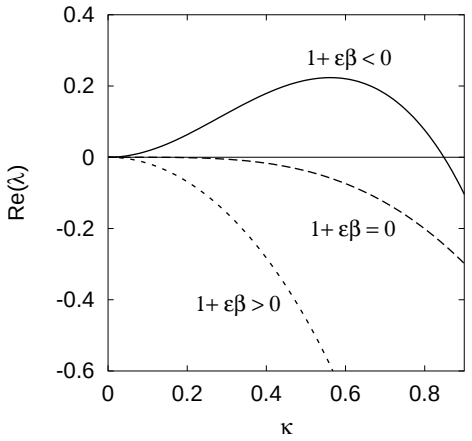

Figure 5.7: Stability of the solution with $\Omega = \omega + \beta$ for a delay of $\tau = 2\pi/(\omega + \beta)$. The real part of λ according to Eq. (5.26) is plotted as a function of wave number κ for three different cases: in the Benjamin-Feir unstable ($1+\varepsilon\beta < 0$) and stable ($1+\varepsilon\beta > 0$) regime and at the border of stability ($1 + \varepsilon\beta = 0$).

are growing, no matter how μ is chosen. Thus, for $1+\varepsilon\beta < 0$ the solution with $\Omega = \omega+\beta$ is always unstable so that a noninvasive stabilization of uniform oscillations with TDAS is not possible in this type of system.

For the solutions with $\Omega \neq \Omega_0$ presented in Fig. 5.6, the feedback signal is non-zero. In this case, μ_c can be determined from the general expression (5.23) for λ by numerically solving Eqs. (5.24) and (5.25). Figure 5.8 shows the critical feedback intensity μ_c as a function of the dispersion parameter ε for $\tau = T_0$ and the other parameters chosen as in Fig. 5.6. In the Benjamin-Feir unstable regime, μ_c lies above the bifurcation point μ_0, at which the solution with $\Omega = \Omega_0$ becomes unstable. As the Benjamin-Feir line is approached with decreasing ε, the critical feedback intensity necessary to stabilize uniform oscillations decreases and finally converges towards μ_0.

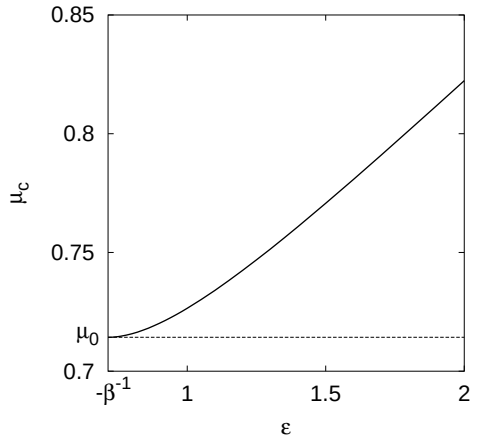

Figure 5.8: Critical feedback intensity μ_c for $\tau = T_0 = 1$ as a function of the dispersion coefficient ε with $\beta = -1.4$. The line $\mu = \mu_0$ denotes the feedback intensity for which the transcritical bifurcation occurs in the uniform system (cf. Fig. 5.6). The other parameters are as in Fig. 5.5 [220].

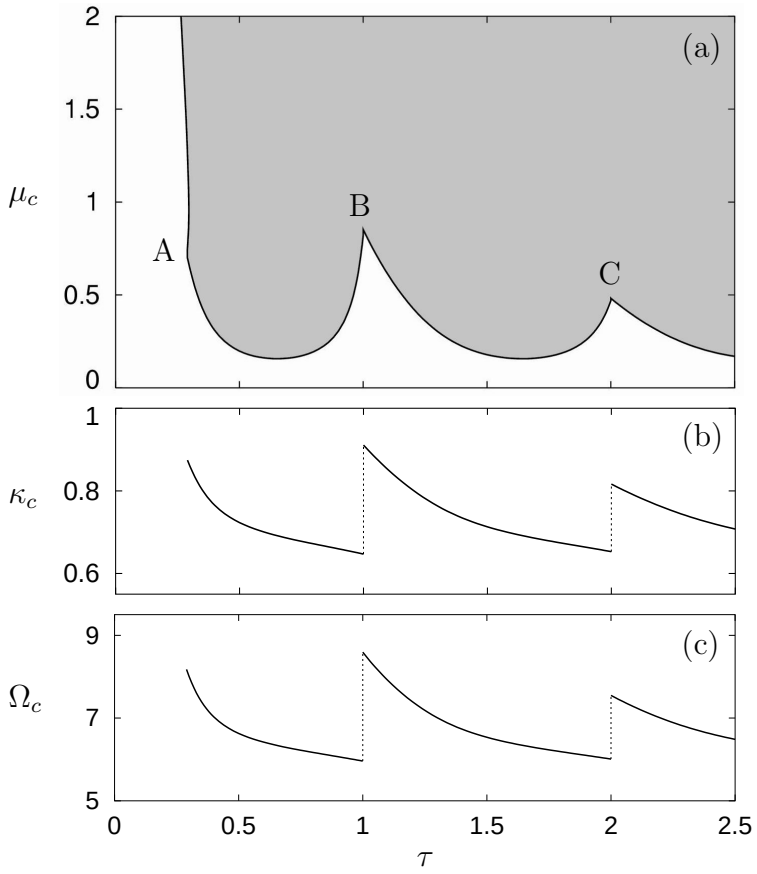

Figure 5.9: (a) Synchronization diagram. Uniform oscillations are stable inside the shaded region. (b,c) The dependences of the critical wave number κ_c and the critical frequency Ω_c on the delay time τ. The parameters are $\varepsilon = 2$, $\beta = -1.4$, $\omega = 2\pi - \beta \approx 7.68$, and $\chi = \pi/2$ [220].

Synchronization diagram From the conditions (5.24) and (5.25), the critical feedback intensity μ_c can be determined as a function of the delay time τ. The resulting synchronization diagram in the plane spanned by the feedback parameters τ and μ is displayed in Fig. 5.9 (a). The curve of the critical feedback intensity μ_c divides the plane into a shaded region, where uniform oscillations are linearly stable with respect to small perturbations of arbitrary wave number, and a region where uniform oscillations are unstable. The boundary between the two regions is characterized by the repeated appearance of cusps. They are observed whenever τ becomes equal to an integer multiple of the period of the unperturbed uniform system, $\tau = k\,2\pi/(\omega+\beta), k = 1, 2, 3, \ldots$. This feature seems to be common for various oscillatory systems with delayed feedback and has also been found in the case of the Kuramoto model of phase oscillators with a delayed global coupling [221]. Figure 5.10 shows an extension of the top part of Fig. 5.9 towards large delay times. With increasing τ, the cusps get less pronounced and the boundary converges to a flat line at $\mu \approx 0.16$.

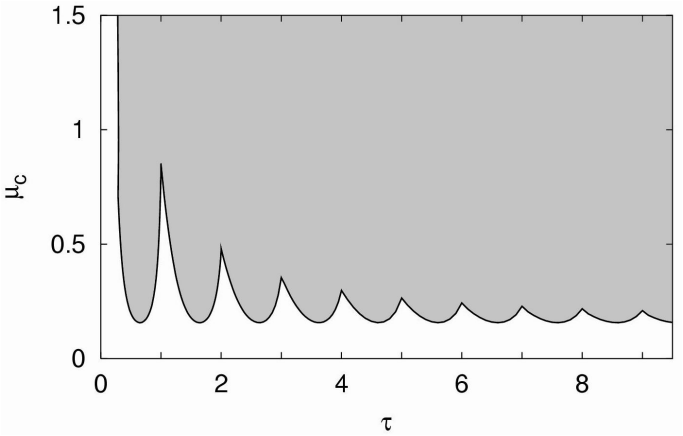

Figure 5.10: Extended synchronization diagram. The same parameters as in Fig. 5.9 [220].

According to the analytically derived synchronization diagram, stability of uniform oscillations can also be maintained by applying global feedbacks with very large delay times. Moreover, the critical feedback strength, needed to maintain synchronization, does not depend on the delay in the limit $\tau \to \infty$. To understand this result, we note that the feedback signal $F(t)$ for $\tau \to \infty$ is given by

$$F(t) = \mu e^{i\chi} \left[\rho_0 e^{-i(\Omega t+\phi_0)} - \bar{\eta}(t)\right] \tag{5.28}$$

where ϕ_0 is a constant phase shift. The first term on the right hand side corresponds to the state $\bar{\eta}(t-\tau)$ at $\tau \to \infty$ which essentially is the initial state of the system. Since the stability boundary is derived for destabilization of initially uniform oscillations, this initial state represents uniform oscillations with frequency Ω and amplitude ρ_0. Substituting the expression (5.28) for $F(t)$ into Eq. (5.11), we see that a situation with external periodic forcing is effectively realized. The critical value μ_c corresponds in this case to the minimum forcing intensity needed to maintain uniform oscillations in the system.

In Fig. 5.9 (b) and (c), the critical wave number and frequency are shown, respectively, as functions of the delay time along the lower part ABC of the stability boundary. The two curves are of similar shape: they display a decrease for increasing delay time interrupted by discontinuous jumps. These discontinuities occur at the locations where the cusps are found in the stability boundary in Fig. 5.9 (a).

In Fig. 5.11, the real part of λ as a function of κ is shown at three different points on the stability curve in the (μ, τ) plane. The three cases correspond to what has been

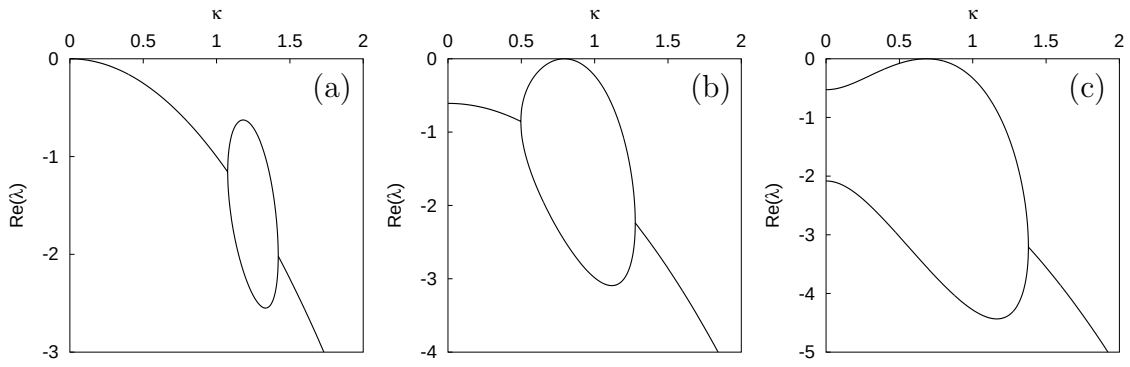

Figure 5.11: Growth rate $\mathrm{Re}\,\lambda$ of spatially nonuniform modes as a function of wave number κ at three different points on the stability curve displayed in Fig. 5.9 (a). The parameters are (a) $\tau = 0.29$, $\mu = 1.29$, (b) $\tau = 0.36$, $\mu = 0.4$, and (c) $\tau = 0.7$, $\mu = 0.16$; other parameters as in Fig. 5.9 [220].

found earlier for a different global delayed feedback scheme in the CGLE [81]. On the branch AB (and similarly also on the branches BC and to the right of C), the first unstable modes occur with a wave number $\kappa_0 \neq 0$ where $\mathrm{Im}(\lambda) = 0$, see Fig. 5.11 (b) and (c). Thus, if we cross this branch of the stability boundary by reducing the feedback intensity below the critical value μ_c, uniform oscillations will become unstable and standing waves with wave number κ_0 will emerge (cf. the following section). A different situation is encountered on the branch reaching from A upwards, see Fig. 5.11 (a). Here, the instability will occur by periodic spatiotemporal modulations of uniform oscillations, since $\mathrm{Im}(\lambda) \neq 0$ and the most unstable modes will have wave numbers close to $\kappa_0 = 0$.

5.2.2 Numerical simulations

Numerical simulations of Eqs. (5.11) and (5.12) are performed to confirm the analytical results. Moreover, the behavior of the system is explored under conditions that are not accessible by analytic arguments. All simulations were carried out for a one-dimensional system. The set of parameters is as in the previous section: $\varepsilon = 2$, $\beta = -1.4$, $\omega = 2\pi - \beta \approx 7.68$, and $\chi = \pi/2$. The choice of the initial conditions and the feedback parameters μ and τ is different for the various simulations and will be specified below.

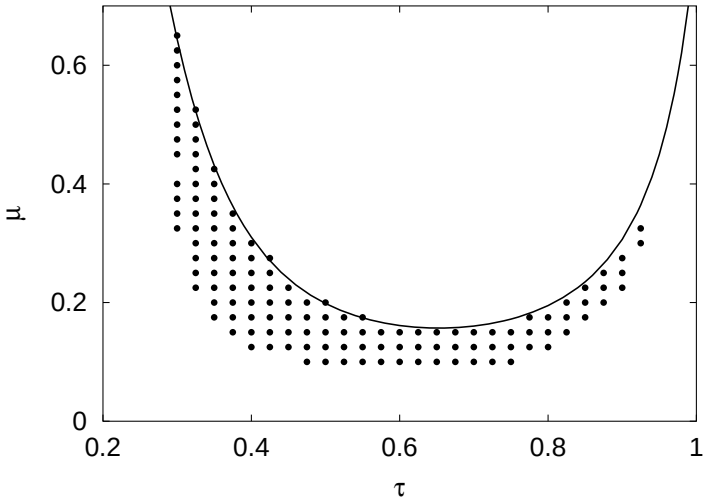

Figure 5.12: Regular patterns at the border of synchronization, uniform initial conditions. Bold dots mark parameters where regular space-time patters are observed. The analytical result of the stability curve (AB branch, solid line) is shown for comparison (cf. Fig. 5.9). Numerical parameters: system length $L = 128$ (1D, periodic boundaries), 400 grid points, time step $\Delta t = 0.001$ [220].

Uniform initial conditions In the first series of simulations, the parameters μ and τ are systematically scanned in steps of $\Delta\mu = \Delta\tau = 0.1$ between 0 and 2.5, respectively, to verify the shape of the stability domain in the (μ, τ) plane. When starting from uniform initial conditions, the stability diagram displayed in Fig. 5.9 (a) is nicely reproduced after transients. Asymptotic states are uniform inside the domain of stability and nonuniform outside this region. These nonuniform states are, however, of different type. Far from the region of stability, we asymptotically reach a fully developed state of defect-mediated turbulence. As the stability boundary is approached, phase turbulence and standing wave patterns are observed close to the branches AB, BC, and to the right of C.

Figure 5.12 shows the results of a more detailed scan of μ and τ in the vicinity of the branch AB of the synchronization diagram in Fig. 5.9 (a). Starting again from uniform initial conditions, the feedback parameters μ and τ are changed in steps of $\Delta\mu = \Delta\tau = 0.025$ between $\tau = 0.25 \ldots 0.975$ and $\mu = 0 \ldots 0.7$. Simulations that, after transients, resulted in a regular nonuniform spatiotemporal state are marked by bold dots at the corresponding (μ, τ) coordinates (simulations leading to uniformly oscillating or turbulent asymptotic states are not shown). Obviously, the parameter region, where regular spatiotemporal patterns occur, constitutes a slightly asymmetric prolongation of the tongue-shaped stability domain for uniform oscillations towards smaller feedback intensities. From the result of the first coarse parameter scan it can be conjectured that the regions where spatiotemporal patterns occur look qualitatively similar at the other tongue-shaped branches of the stability curve.

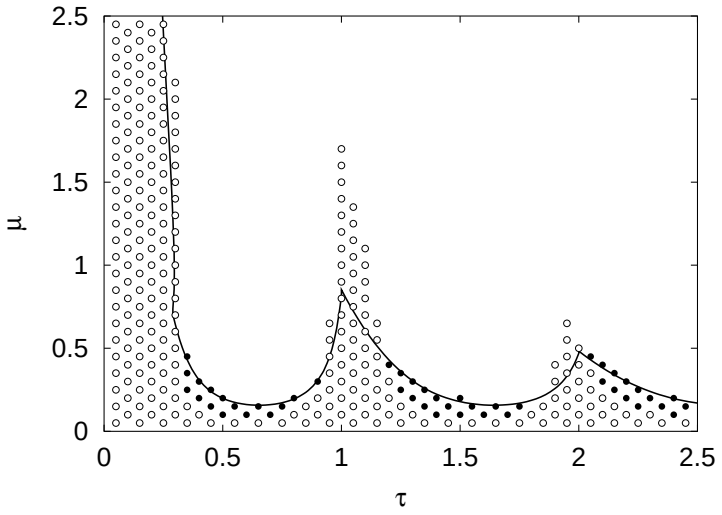

Figure 5.13: Simulations starting from turbulent initial conditions. Amplitude turbulence (open circles), regular nonuniform patterns (bold circles), and uniform oscillations (no symbols) are distinguished. The analytically derived stability boundary for uniform initial conditions (solid line) is shown for comparison. For model and numerical parameters see Figs. 5.9 and 5.12, respectively [220].

Turbulent initial conditions When starting from turbulent initial conditions, the stability boundary for uniform oscillations is moved towards larger feedback intensities in the vicinity of the cusps. The results of numerical simulations are summarized in Fig. 5.13. Here, open circles indicate a turbulent asymptotic state and bold circles again denote the appearance of a regular nonuniform wave pattern. Inside the area where no symbols are shown, simulations converge towards uniform oscillations. For comparison, the analytically derived synchronization diagram from Fig. 5.9 (a) is also displayed.

Spatiotemporal patterns In the parameter range between turbulence and uniform oscillations, different patterns can be observed. In Fig. 5.14, a series of space-time plots of asymptotic dynamical states reached for different feedback intensities is shown. At a fixed delay time of $\tau = 0.5$, the feedback intensity μ is increased in Fig. 5.14 from (a) to (e). In absence of feedback (Fig. 5.14 (a), $\mu = 0$) and for small feedback intensities (Fig. 5.14 (b), $\mu = 0.05$), an irregular state of defect-mediated turbulence is observed. However, the number of defects is smaller in the presence of a weak feedback and the time evolution shows intervals where almost no defects are seen. If the feedback intensity is increased (Fig. 5.14 (c), $\mu = 0.07$), defects are no longer observed and the system displays a disordered state of phase turbulence. For even stronger feedback, breathing (Fig. 5.14 (d), $\mu = 0.1$) and stationary standing wave patterns (Fig. 5.14 (e), $\mu = 0.15$) can be observed. For still larger feedbacks, $\mu > 0.2$ (not shown), uniform oscillations take place.

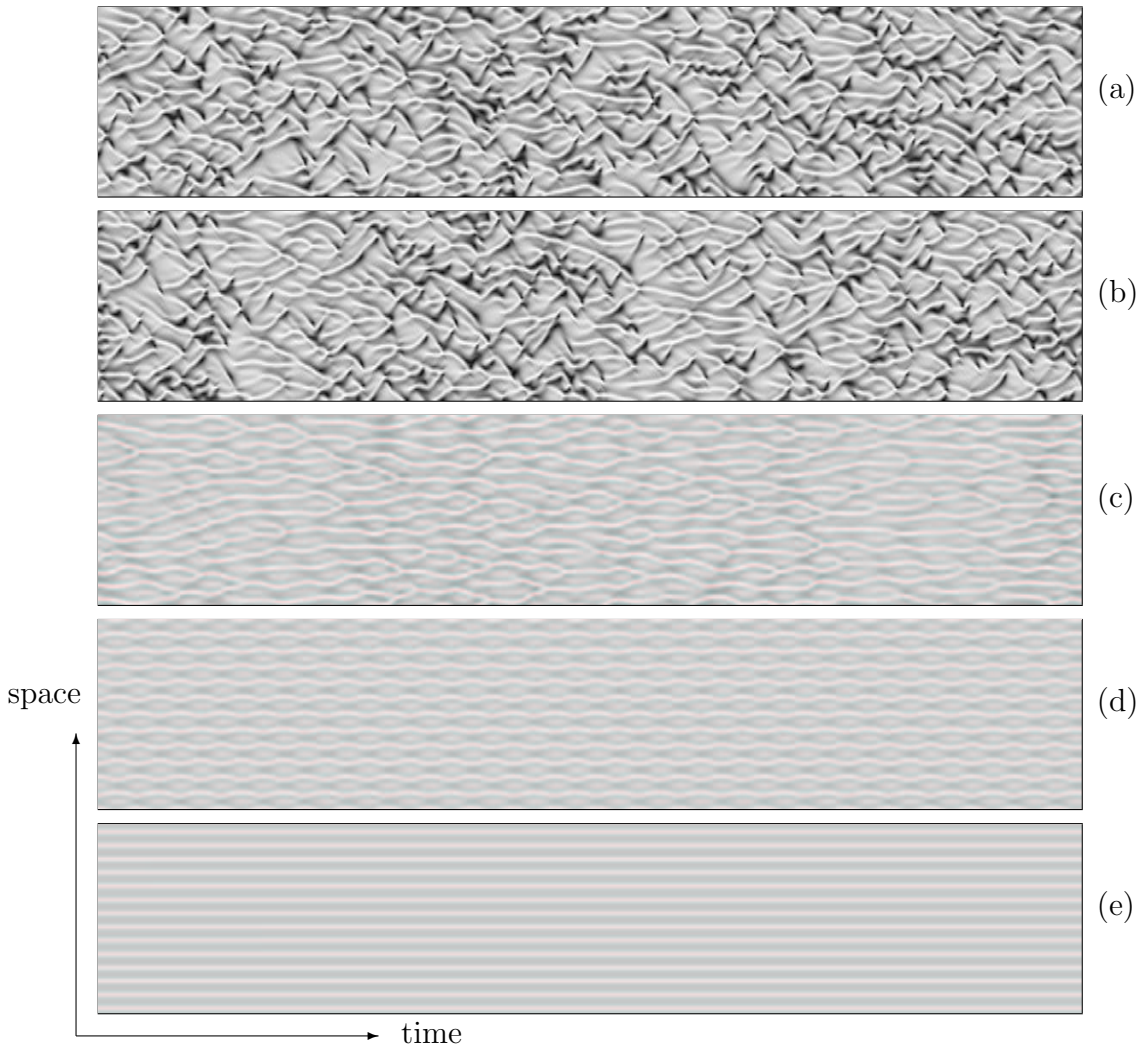

Figure 5.14: Spatiotemporal patterns in the parameter region between turbulence and complete synchronization. The amplitude $|\eta|$ is displayed in a linear gray scale coding between 0 (black) and 1.2 (white). The delay time is kept constant, $\tau = 0.5$ s, and the feedback intensity increases from top to bottom, (a) $\mu = 0$, (b) $\mu = 0.05$, (c) $\mu = 0.07$, (d) $\mu = 0.1$, and (e) $\mu = 0.15$. An interval of 500 time units is displayed. For model and numerical parameters see Figs. 5.9 and 5.12, respectively [220].

Large delay times To study the behavior of the system for large time delays, a series of simulations with the delay τ varying from 0.5 to 29.5 in steps of $\Delta\tau = 1$ has been performed. The feedback intensity μ was varied for each choice of τ from 0.1 to 0.3 in steps of $\Delta\mu = 0.1$. As initial condition, the state of amplitude turbulence was chosen that is established in the system for $\mu = 0$. The simulations have shown that synchronization is possible for all chosen delays when the feedback intensity exceeds

a critical level. In another series of numerical experiments, the feedback intensity was fixed at $\mu = 1$ and the delay time τ was increased from 0 to 50 in steps of 0.1. Here, the transient time was determined for each of the simulations by measuring the convergence of the statistical variance of the amplitude ρ. It was found that for small delays the transient time increases proportionally to the delay τ. For delays larger than $\tau = 5$, the transient time undergoes saturation showing modulations around a constant level that depends only on the intensity of the applied feedback.

For long delays τ, the component $\bar{\eta}(t - \tau)$ in the feedback signal $F(t)$ at time t corresponds to the initial state of amplitude turbulence. Thus, the global delayed feedback scheme in the considered limit effectively represents global forcing of the system with an external chaotic signal. To verify this conjecture, special numerical simulations have been performed. In these simulations, the feedback signal was generated by replacing $\bar{\eta}(t - \tau)$ with the average complex oscillation amplitude of the same system without feedback. It was found that, by applying such chaotic external forcing, synchronization of uniform oscillations can also be achieved.